Earthq Eng & Eng Vib (2014) 13: 731-740 **DOI**: 10.1007/s11803-014-0276-3

Dynamic analysis of slab track on multi-layered transversely isotropic saturated soils subjected to train loads

Zhan Yongxiang[1, 2†], Yao Hailin[1, 2‡], Lu Zheng[1, 2§] and Yu Dongming[1, 2†]

1. *Institute of Rock and Soil Mechanics, Chinese Academy of Sciences, Wuhan 430071, China*
2. *State Key Laboratory of Geomechanics and Geotechnical Engineering, Institute of Rock and soil Mechanics, Chinese Academy of Sciences, Wuhan 430071, China*

Abstract: The dynamic responses of a slab track on transversely isotropic saturated soils subjected to moving train loads are investigated by a semi-analytical approach. The track model is described as an upper Euler beam to simulate the rails and a lower Euler beam to model the slab. Rail pads between the rails and slab are represented by a continuous layer of springs and dashpots. A series of point loads are formulated to describe the moving train loads. The governing equations of track-ground systems are solved using the double Fourier transform, and the dynamic responses in the time domain are obtained by the inverse Fourier transform. The results show that a train load with high velocity will generate a larger response in transversely isotropic saturated soil than the lower velocity load, and special attention should be paid on the pore pressure in the vicinity of the ground surface. The anisotropic parameters of a surface soil layer will have greater influence on the displacement and excess pore water pressure than those of the subsoil layer. The traditional design method taking ground soil as homogeneous isotropic soil is unsafe for the case of RE < 1 and RG < 1, so a transversely isotropic foundation model is of great significance to the design for high train velocities.

Keywords: slab track; transversely isotropic saturated soil; Biot's theory; train load; dynamic response

1 Introduction

In a number of engineering fields such as civil engineering, transportation engineering and environmental engineering, much attention has been paid on the studies of the dynamic responses of railway tracks and the adjoining ground under the action of moving trains. With the development of even faster trains, excessive ground vibration becomes an increasing concern when the ground consists of soft materials such as various types of clay.

In these materials, the Rayleigh-wave velocity may even be lower than modern high train velocities. Some existing works indicated that when the train velocity approaches the Rayleigh-wave velocity of the soil, the ground and the rails show significant vibration, thus it is important to study the dynamic responses of track systems on soft clay under moving train loads.

Vibration of a track system on the ground was first proposed by Kennedy and Herrmann (1973a, 1973b) who gave an analytical solution for a visco-elastic ground matrix under moving point loads. Biot (1956, 1962) pioneered the development of an elastodynamic theory for fluid-filled elastic porous media. Later, many researchers (Burke and Kingsbury, 1984; Siddharthan *et al.*, 1993; Theodorakopoulos, 2003; Jin, 2004; Lu and Jeng, 2007; Cai *et al.*, 2008; Ling *et al.*, 2009; Bian *et al.*, 2010) applied Biot's theory to deal with the dynamic responses of a fully water-saturated soil under moving loads and studied the dynamic responses of a track-ground system subjected to train loads using a sandwich beam-structure track model. The effects of the characteristics of poroelastic soil media on the dynamic responses were studied in detail. Results show that the dynamic characteristics of poroelastic soil media were quite different from those of the elastic soil media when the train speed exceeded the critical velocity of the track-ground system.

In fact many materials in geotechnical engineering are multi-layered and transversely isotropic. For example, natural soil and rock are often formed through a sedimentation process and have different mechanical properties in different directions. Compared with a uniform elastic material model, using a multi-layered

Correspondence to: Zhan Yongxiang, Institute of Rock and Soil Mechanics, Chinese Academy of Sciences, Wuhan 430071, China
Tel: +86-27-87198350;
E-mail: zhanyongxiang@126.com
†Assistant Professor; ‡Professor; §Associate Professor

Supported by: the National Basic Research Program of China under Grant No. 2013CB036405, the Key Research Program of the Chinese Academy of Sciences under Grant No. KZZD-EW-05, and the Natural Science Foundation of China under Grant Nos. 41402317, 51209201 and 51279198
Received April 9, 2013; **Accepted** January 15, 2014

transversely isotropic model to describe the deformation of layered media is more reasonable. Many researchers conducted numerous studies on this topic (Yue, 1995; Chen *et al.*, 1998; Abousleiman and Cui, 1998; Rahman and Newaz, 2000; Yu, 2001; Wang *et al.*, 2006). However, the major limitation of these works lies in that the dynamic wheel-rail force was not considered in these investigations, and the study of dynamic responses of slab tracks on multi-layered transversely isotropic saturated soils subjected to train loads was rarely reported.

In this paper, the dynamic responses of slab tracks on transversely isotropic saturated soils subjected to moving train loads are investigated by a semi-analytical approach. The track model is described as an upper Euler beam to simulate the rails and a lower Euler beam to model the slab. Rail pads between the rails and slab are represented by a continuous layer of springs and dashpots. It is assumed that the interface of the slab and the transversely isotropic saturated soil medium is permeable. A series of point loads are formulated to describe the moving train loads. The governing equations of track-ground systems are solved using the double Fourier transform, while the dynamic responses in the time domain are obtained by the inverse Fourier transform. The effects of the moving load velocity and anisotropic parameters on soil dynamic response have been carefully analyzed.

2 Governing equations and general solutions

2.1 Analytical solution of transversely isotropic saturated soils

The model of slab-track-ground coupling system is shown in Fig. 1. The coordinate system is taken to be a rectangular Cartesian with the z-axis pointing vertically downward. The ground surface is located at $z = 0$, and the x-axis is taken in the direction of movement of a train load. According to the theory of Biot (1962) and transversely isotropic elasticity, the governing equations of transversely isotropic saturated soil can be expressed as follows:

$$\left.\begin{aligned}
&C_{11}\frac{\partial^2 u_1}{\partial x_1^{\,2}}+C_{66}\frac{\partial^2 u_1}{\partial y^2}+C_{44}\frac{\partial^2 u_1}{\partial z^2}+(C_{12}+C_{66})\frac{\partial^2 u_2}{\partial x_1\partial y}+\\
&(C_{13}+C_{44})\frac{\partial^2 u_3}{\partial x_1\partial z}-\alpha\frac{\partial p}{\partial x_1}=\rho\ddot{u}_1+\rho_{\mathrm{f}}\ddot{w}_1\\
&C_{66}\frac{\partial^2 u_2}{\partial x_1^{\,2}}+C_{11}\frac{\partial^2 u_2}{\partial y^2}+C_{44}\frac{\partial^2 u_2}{\partial z^2}+(C_{12}+C_{66})\frac{\partial^2 u_1}{\partial x_1\partial y}+\\
&(C_{13}+C_{44})\frac{\partial^2 u_3}{\partial y\partial z}-\alpha\frac{\partial p}{\partial y}=\rho\ddot{u}_2+\rho_{\mathrm{f}}\ddot{w}_2\\
&C_{44}\frac{\partial^2 u_3}{\partial x_1^{\,2}}+C_{44}\frac{\partial^2 u_3}{\partial y^2}+C_{33}\frac{\partial^2 u_3}{\partial z^2}+(C_{13}+C_{44})\frac{\partial^2 u_1}{\partial x_1\partial z}+\\
&(C_{13}+C_{44})\frac{\partial^2 u_2}{\partial y\partial z}-\alpha\frac{\partial p}{\partial z}=\rho\ddot{u}_3+\rho_{\mathrm{f}}\ddot{w}_3
\end{aligned}\right\}\quad(1)$$

where:

$$\begin{aligned}
C_{11}&=E_{\mathrm{H}}(1-\mu_{\mathrm{HV}}^2\cdot E_{\mathrm{H}}/E_{\mathrm{V}})/(1+\mu_{\mathrm{HH}})\Delta\\
C_{12}&=E_{\mathrm{H}}(\mu_{\mathrm{HH}}+\mu_{\mathrm{HV}}^2\cdot E_{\mathrm{H}}/E_{\mathrm{V}})/(1+\mu_{\mathrm{HH}})\Delta\\
C_{13}&=E_{\mathrm{H}}\mu_{\mathrm{HV}}/\Delta\\
C_{33}&=E_{\mathrm{V}}(1-\mu_{\mathrm{HH}})/\Delta\\
C_{44}&=G_{\mathrm{V}}\\
C_{66}&=E_{\mathrm{H}}/2(1+\mu_{\mathrm{HH}})\\
\Delta&=1-\mu_{\mathrm{HH}}-2\mu_{\mathrm{HV}}^2\cdot E_{\mathrm{H}}/E_{\mathrm{V}}\\
E_{\mathrm{H}}\mu_{\mathrm{VH}}&=E_{\mathrm{V}}\mu_{\mathrm{HV}}
\end{aligned}$$

C_{ij} (i, j = 1–6) are elastic constants of the transversely isotropic saturated medium; E_{V} and E_{H} are Young′s modulus in the vertical and horizontal direction respectively; G_{V} is the shear modulus in planes normal to the plane of transverse isotropy; μ_{HH} and μ_{HV} are Poisson′s ratios characterizing the lateral strain response in the plane of transverse isotropy to a stress acting parallel and normally to the plane respectively; u_i and w_i (i = 1, 2, 3) are the soil skeleton displacement components and pore fluid average displacement relative to soil skeleton displacement along the x, y, z directions respectively; dots on u_i and w_i indicate the differential with respect to time t; $\rho = n\cdot\rho_{\mathrm{f}} + (1\text{-}n)\rho_{\mathrm{s}}$, where ρ_{s} and ρ_{f} are the mass densities of solid skeletons and pore fluids respectively, and n is the porosity of porous soil media.

The seepage continuous equation is given as:

$$p=-M\dot{w}_{i,i}-\alpha M\dot{u}_{i,i}\quad(2)$$

The fluid motion equation is as follows:

$$p_{,i}=-\rho_{\mathrm{f}}\ddot{u}_i-m\ddot{w}_i-b\,\dot{w}_i\quad(3)$$

where, p is the excess pore water pressure; M and α are Biot's parameters accounting for the compressibility of the two-phase material, $0 \le M \le \infty$, $0 \le \alpha \le 1$; m is a density-like parameter that depends on ρ_{f} and the geometry of the pores; b is a parameter accounting for the internal friction due to the relative motion between the solid and the pore fluid. The parameter $b = \eta_{\mathrm{w}}/k_{\mathrm{s}}$ is the ratio of the fluid viscosity to the intrinsic permeability of the medium.

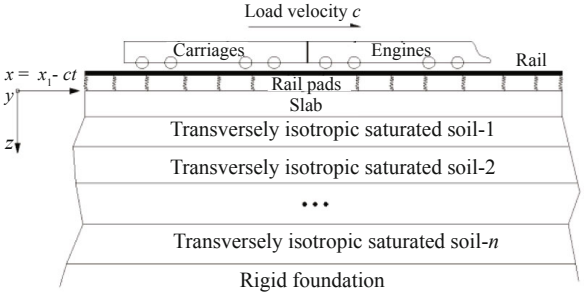

Fig. 1 The model of slab-track-ground coupling system

A moving coordinate can be defined as $x = x_1 - ct$, $y = y$, $z = z$, in which c is the load velocity, and the Fourier transform with respect to the x and y coordinates is defined as:

$$\overline{f}(\zeta,\eta)=\int_{-\infty}^{\infty}\int_{-\infty}^{\infty}f(x,y)\mathrm{e}^{-\mathrm{i}(\zeta x+\eta y)}\mathrm{d}x\mathrm{d}y \tag{4}$$

and the inverse relationship is given by the following form:

$$f(x,y)=\frac{1}{4\pi^2}\int_{-\infty}^{\infty}\int_{-\infty}^{\infty}\overline{f}(\zeta,\eta)\mathrm{e}^{\mathrm{i}(\zeta x+\eta y)}\mathrm{d}\zeta\,\mathrm{d}\eta \tag{5}$$

where, ζ and η are wave numbers in the x and y directions, f is a variable in the space domain, and $\overline{f}$ is the corresponding variable in the transformed domain. In fixed coordinate system, for the train load form $\delta(x_1\text{-}ct)\cdot P_0\cdot\mathrm{e}^{\mathrm{i}\omega t}$, the response function after the Fourier transformation can be expressed as:

$$\varphi(\zeta,\eta,z,t)=\varphi(\zeta,\eta,z)\mathrm{e}^{\mathrm{i}(\omega-\zeta c)t} \tag{6}$$

where, P_0 is the axle load of the train, ω is the circular frequency, and then ω is set as zero, because in the paper the effects of circular frequency on dynamic response was not studied.

Performing the Fourier transform with respect to the x and y on Eqs. (1)–(3), by introducing the variable as $\overline{e}_{\mathrm{h}}=\zeta\overline{u}_1+\eta\overline{u}_2$ and $\beta = 1/(m\Omega^2\text{-i}\Omega b)$, in which $\Omega = \omega - c\zeta$, and after eliminating u_1 and u_2, we obtain:

$$\begin{bmatrix}C_{44}&&\\&C_{33}&\\&&M\beta\end{bmatrix}\frac{\partial^2}{\partial z^2}\begin{bmatrix}\overline{e}_h\\\overline{u}_3\\\overline{p}\end{bmatrix}+\begin{bmatrix}&b_1&\\b_2&&b_3\\&b_4&\end{bmatrix}\frac{\partial}{\partial z}\begin{bmatrix}\overline{e}_h\\\overline{u}_3\\\overline{p}\end{bmatrix}+\begin{bmatrix}b_5&&b_6\\&b_7&\\b_8&&b_9\end{bmatrix}\begin{bmatrix}\overline{e}_h\\\overline{u}_3\\\overline{p}\end{bmatrix}=\begin{bmatrix}0\\0\\0\end{bmatrix} \tag{7}$$

where:

$b_1 = (\text{-}C_{13}\mathrm{i} - C_{44}\mathrm{i})(\zeta^2+\eta^2)$

$b_2 = \text{-}C_{44}\mathrm{i} - C_{13}\mathrm{i}$

$b_3 = \beta\Omega^2\rho_{\mathrm{f}} - \alpha$

$b_4 = \alpha M - \rho_{\mathrm{f}}\beta M\Omega^2$

$b_5 = \text{-}C_{11}\zeta^2 - C_{11}\eta^2 + \rho\Omega^2 - \rho_{\mathrm{f}}^2\beta\Omega^4$

$b_6 = (\mathrm{i}\alpha - \mathrm{i}\rho_{\mathrm{f}}\beta\Omega^2)(\zeta^2+\eta^2)$

$b_7 = \text{-}C_{44}\zeta^2 - C_{44}\eta^2 + \rho\Omega^2 - \rho_{\mathrm{f}}^2\beta\Omega^4$

$b_8 = \mathrm{i}M\rho_{\mathrm{f}}\beta\Omega^2 - \mathrm{i}\alpha M$

$b_9 = 1 - \beta M(\zeta^2+\eta^2)$

The solution of Eq. (7) can be assumed as:

$$\left[\overline{e}_{\mathrm{h}}\quad\overline{u}_3\quad\overline{p}\right]^{\mathrm{T}}=\left[C_1\quad C_2\quad C_3\right]^{\mathrm{T}}\exp(\lambda z) \tag{8}$$

Substituting Eq. (8) into Eq. (7), the characteristic equation can be obtained:

$$a_1\lambda^6+a_2\lambda^4+a_3\lambda^2+a_4=0 \tag{9}$$

where:

$a_1 = C_{33}C_{44}M\beta$

$a_2 = C_{33}C_{44}b_9+b_7C_{44}M\beta\text{-}C_{44}b_3b_4+C_{33}b_5M\beta\text{-}b_1b_2M\beta$

$a_3 = C_{44}b_7b_9+C_{33}b_5b_9+b_5b_7M\beta\text{-}b_3b_4b_5+b_1b_3b_8\text{-}b_1b_2b_9+b_2b_4b_6\text{-}C_{33}b_6b_8$

$a_4 = b_5b_7b_9 - b_6b_7b_8$

Equation (9) is a 6-th degree equation in one variable with complex coefficients, which has six characteristic roots that can be defined as λ_1, λ_2, λ_3, λ_4, λ_5 and λ_6. The solutions of the characteristic roots can be obtained by using a Matlab program to give Eq. (8) that can be expressed as:

$$\left.\begin{aligned}\overline{e}_{\mathrm{h}}&=\sum_{s=1}^{6}C_s h_s\mathrm{e}^{\lambda_s z}\\\overline{u}_3&=\sum_{s=1}^{6}C_s r_s\mathrm{e}^{\lambda_s z}\\\overline{p}&=\sum_{s=1}^{6}C_s\mathrm{e}^{\lambda_s z}\end{aligned}\right\} \tag{10}$$

where C_s (s = 1, 2, … , 6) are undetermined coefficients.

$$h_s=\frac{-b_1\lambda_s r_s-b_6}{C_{44}\lambda_s^2+b_5}$$

$$r_s=\frac{b_2b_6\lambda_s-b_3\lambda_s(C_{44}\lambda_s^2+b_5)}{(C_{33}\lambda_s^2+b_7)(C_{44}\lambda_s^2+b_5)-b_1b_2\lambda_s^2}$$

In view of the relationship of $\overline{e}_{\mathrm{h}}$, $\overline{u}_1$ and $\overline{u}_2$, $\overline{u}_1$ can be obtained by:

$$\overline{u}_1=\sum_{s=1}^{6}C_s W_s\mathrm{e}^{\lambda_s z} \tag{11}$$

where:

$$W_s=(C_{13}\mathrm{i}\zeta\lambda_s r_s+C_{44}\mathrm{i}\zeta\lambda_s r_s+C_{12}\zeta h_s+C_{66}\zeta h_s-\alpha\mathrm{i}\zeta+\mathrm{i}\rho_{\mathrm{f}}\beta\zeta\Omega^2)/(C_{44}\lambda_s^2+C_{12}\zeta^2+C_{66}\zeta^2-C_{11}\zeta^2-C_{66}\eta^2+\rho\Omega^2-\rho_{\mathrm{f}}^2\beta\Omega^4)$$

The constitutive relationship of saturated soil can be expressed as:

$$\sigma_{33}=C_{13}(u_1+u_2)+C_{33}u_3-\alpha p \tag{12}$$

$$\sigma_{13}=C_{44}\left(\frac{\partial u_1}{\partial z}+\frac{\partial u_3}{\partial x}\right) \tag{13}$$

According to the constitutive relationship Eqs. (12)–(13), by using the Fourier transform, the following equations are obtained:

$$\overline{\sigma}_{33} = \sum_{s=1}^{6} C_s N_s \mathrm{e}^{\lambda_s z} \tag{14}$$

$$\overline{\sigma}_{13} = \sum_{s=1}^{6} C_s M_s \mathrm{e}^{\lambda_s z} \tag{15}$$

where:

$N_s = -\mathrm{i}C_{13}h_s + C_{33}\lambda_s r_s - \alpha$

$M_s = C_{44}\lambda_s W_s - \mathrm{i}C_{44}\zeta r_s$

Therefore, in the Fourier transform domain, the dynamic response solutions of soil stress, displacement and pore water pressure under moving loads are obtained in transversely isotropic saturated ground.

For a multi-layered ground model, the general solutions of each layer are consistent with the above solutions in the form, while the soil parameters are different. Therefore, the dynamic response solutions of the kth layer soil can be defined as:

$$\left.\begin{aligned}
\overline{u}_1^{(k)} &= \sum_{s=1}^{6} C_s^{(k)} W_s^{(k)} \mathrm{e}^{\lambda_s^{(k)} z} \\
\overline{u}_3^{(k)} &= \sum_{s=1}^{6} C_s^{(k)} r_s^{(k)} \mathrm{e}^{\lambda_s^{(k)} z} \\
\overline{p}^{(k)} &= \sum_{s=1}^{6} C_s^{(k)} \mathrm{e}^{\lambda_s^{(k)} z} \\
\overline{\sigma}_{33}^{(k)} &= \sum_{s=1}^{6} C_s^{(k)} N_s^{(k)} \mathrm{e}^{\lambda_s^{(k)} z} \\
\overline{\sigma}_{13}^{(k)} &= \sum_{s=1}^{6} C_s^{(k)} M_s^{(k)} \mathrm{e}^{\lambda_s^{(k)} z}
\end{aligned}\right\} \tag{16}$$

where $r_s^{(k)}$, $\lambda_s^{(k)}$, $W_s^{(k)}$, $N_s^{(k)}$, $M_s^{(k)}$ (s = 1, 2, … , 6) are the parameters of the kth layer.

2.2 Description of the railway track

The track system used here is introduced from that of Picoux and Le Houedec (2005). The equation for the rails represented by an Euler Beam is written as:

$$\delta_{\mathrm{R}} \frac{\partial^4 u_{\mathrm{R}}(x_1,t)}{\partial x_1^4} + m_{\mathrm{R}} \frac{\partial^2 u_{\mathrm{R}}(x_1,t)}{\partial t^2} + k_{\mathrm{p}}[u_{\mathrm{R}}(x_1,t) - u_{\mathrm{S}}(x_1,t)] + c_{\mathrm{p}}\left[\frac{\partial u_{\mathrm{R}}(x_1,t)}{\partial t} - \frac{\partial u_{\mathrm{S}}(x_1,t)}{\partial t}\right] = \begin{cases} F(x_1,t) & x_1 - ct = 0 \\ 0 & x_1 - ct \neq 0 \end{cases} \tag{17}$$

where u_{R} is the displacement of the Euler beam; δ_{R} is the bending rigidity of the rail; m_{R} is the mass of the rail per unit length; k_{p} and c_{p} denote the spring constant and the damping coefficient of the rail pads, respectively; F is the load acting on the Euler beam; u_{S} is the displacement of the slab and x_1-ct indicates the load position.

The governing equation of the slab is as follows:

$$\delta_{\mathrm{S}} \frac{\partial^4 u_{\mathrm{S}}(x_1,t)}{\partial x^4} + m_{\mathrm{S}} \frac{\partial^2 u_{\mathrm{S}}(x_1,t)}{\partial t^2} - k_{\mathrm{p}}[u_{\mathrm{R}}(x_1,t) - u_{\mathrm{S}}(x_1,t)] - c_{\mathrm{p}}\left[\frac{\partial u_{\mathrm{R}}(x_1,t)}{\partial t} - \frac{\partial u_{\mathrm{S}}(x_1,t)}{\partial t}\right] = -F_{\mathrm{S}}(x_1,t) \tag{18}$$

where δ_{S} is the bending rigidity of the slab; m_{S} is the mass of the slab per unit length; F_{S} is the force between the slab and the soil.

Using Eqs. (4)–(6), the following set of equations relative to the track in the Fourier transformed domain is obtained from Eqs. (17)–(18):

$$A_1(\zeta)\overline{u}_{\mathrm{R}}(\zeta,t) + A_2(\zeta)\overline{u}_{\mathrm{S}}(\zeta,t) = \overline{F}(\zeta,t) \tag{19}$$

$$A_3(\zeta)\overline{u}_{\mathrm{R}}(\zeta,t) + A_4(\zeta)\overline{u}_{\mathrm{S}}(\zeta,t) = -\overline{F}_{\mathrm{S}}(\zeta,t) \tag{20}$$

where:

$A_1(\zeta) = \delta_{\mathrm{R}}\zeta^4 - m_{\mathrm{R}}\Omega^2 + k_{\mathrm{p}} + \mathrm{i}c_{\mathrm{p}}\Omega$

$A_2(\zeta) = -k_{\mathrm{p}} - \mathrm{i}c_{\mathrm{p}}\Omega$

$A_3(\zeta) = A_2(\zeta)$

$A_4(\zeta) = \delta_{\mathrm{S}}\zeta^4 - m_{\mathrm{S}}\Omega^2 + k_{\mathrm{p}} + \mathrm{i}c_{\mathrm{p}}\Omega$

2.3 Description of the train load

In deriving the ground vibration under train passage, a series of moving axle loads are formulated in view of the train geometry in Fig. 2. Here the model of Takemiya and Bian (2005) is employed:

$$F_{\mathrm{T}}(\xi) = \sum_{n=1}^{N_{\mathrm{T}}} (P_{\mathrm{E}}(1 + \mathrm{e}^{\mathrm{i}w_{\mathrm{a}}\xi} + \mathrm{e}^{\mathrm{i}(w_{\mathrm{a}}+w_{\mathrm{b}})\xi} + \mathrm{e}^{\mathrm{i}(2w_{\mathrm{a}}+w_{\mathrm{b}})\xi}) + P_{\mathrm{C}}(1 + \mathrm{e}^{\mathrm{i}w_{\mathrm{a}}\xi} + \mathrm{e}^{\mathrm{i}(w_{\mathrm{a}}+w_{\mathrm{b}})\xi} + \mathrm{e}^{\mathrm{i}(2w_{\mathrm{a}}+w_{\mathrm{b}})\xi})\mathrm{e}^{\mathrm{i}(n-1)L_{\mathrm{C}}\xi}\mathrm{e}^{\mathrm{i}(d_{\mathrm{t}}+L_{\mathrm{E}})\xi})\mathrm{e}^{\mathrm{i}L_{\mathrm{Dis}}\xi} \tag{21}$$

where, P_{E} and P_{C} are the axle loads of the engines and the carriages respectively; N_{T} is the number of the carriages; L_{E} and L_{C} are the engine length and carriage length, respectively; w_{a} is the distance between the first and second axles of a carriage; w_{b} is the distance between the second and third axles of a carriage; d_{t} is the distance between the first axle of a carriage and the end of the former carriage; L_{Dis} is the distance between the

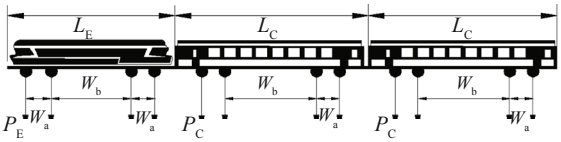

Fig. 2 The train load model

train and the observation point. The parameters of a train are given in Table 1, in which three carriages and one engine are taken into account for the train.

2.4 Boundary conditions

It is assumed that the interface of the slab and the transversely isotropic saturated soil medium is permeable, there is complete contact between the adjacent layers, and that the last layer at the bottom of transversely isotropic saturated soils is a rigid impermeable foundation. The boundary conditions for the problem may then be taken as:

$$\left.\begin{aligned}
&\bar{\sigma}_{33}^{(1)}\big|_{z=0}=-\frac{\bar{F}_{\mathrm{s}}\sin\eta L}{\eta L},\ \bar{u}_3^{(1)}\big|_{z=0}=\bar{u}_{\mathrm{s}},\ \bar{\sigma}_{13}^{(1)}\big|_{z=0}=0\\
&\bar{p}^{(1)}\big|_{z=0}=0\\
&\bar{\sigma}_{33}^{(k)}=\bar{\sigma}_{33}^{(k+1)},\ \bar{\sigma}_{13}^{(k)}=\bar{\sigma}_{13}^{(k+1)},\ \bar{u}_1^{(k)}=\bar{u}_1^{(k+1)},\\
&\bar{u}_3^{(k)}=\bar{u}_3^{(k+1)},\ \bar{p}^{(k)}=\bar{p}^{(k+1)},\ \frac{\partial\bar{p}^{(k)}}{\partial z}=\frac{\partial\bar{p}^{(k+1)}}{\partial z}\\
&\bar{u}_1^{(n)}\big|_{z=H}=0,\ \bar{u}_3^{(n)}\big|_{z=H}=0,\ \frac{\partial\bar{p}^{(n)}}{\partial z}\big|_{z=H}=0
\end{aligned}\right\}\quad(22)$$

where, H is the total height of the multi-layered transversely isotropic saturated soil, and L is the width of the half slab.

Substituting the general solutions of the dynamic responses into Eq. (22), we can obtain the parameters $C_i^{(k)}$ (i = 1, 2, … , 6; k = 1, 2, … , n). By performing the inverse Fourier transform, the dynamic response solutions of the foundation in transversely isotropic saturated layered ground can be obtained as follows:

$$(u_3^{(k)},p^{(k)})=\frac{1}{4\pi^2}\int_{-\infty}^{\infty}\int_{-\infty}^{\infty}(\bar{u}_3^{(k)},\bar{p}^{(k)})\mathrm{e}^{\mathrm{i}(\zeta x+\eta y)}\mathrm{d}\zeta\,\mathrm{d}\eta\quad(23)$$

In this study, the fast Fourier transform (FFT) will be used to perform the inverse transform with respect to ζ and η. To compute the inverse transform accurately with a discrete transform, the integrals must be truncated at sufficiently high values to avoid distortion of the results, while the mesh of the calculated functions must be fine enough to well represent the details of the functions. According to Takemiya and Bian (2005), an FFT algorithm is employed with a grid of 1024×1024 points with a range of -4 m^{-1} < ζ < 4 m^{-1} and -4 m^{-1} < η < 4 m^{-1} to satisfy both these requirements. The amplitude of displacements and excess pore water pressures in the following parts are defined as F = sqrt[Re(F)^2+Im(F)^2]. The transversely isotropic foundation is considered as a double layer and the heights of the two layers are both 8 m. The slab track and soil properties are presented in Table 2.

3 Numerical results and discussion

3.1 Verification

The anisotropic parameters $R_{\mathrm{E}}=E_{\mathrm{H}}/E_{\mathrm{V}}$, $R_{\mathrm{G}}=C_{66}/G_{\mathrm{V}}$ and $R_{\mu}=\mu_{\mathrm{HH}}/\mu_{\mathrm{HV}}$ are introduced to represent the degree of anisotropy for the elastic modulus, shear modulus and Poisson ratio in the horizontal and vertical directions, respectively. Thus when R_{E} = 1, R_{G} = 1 and R_{μ} = 1, the ground soil becomes isotropic. In order to verify the accuracy of the present procedure on further application to the train load, Fig. 3 compares the numerical result of the vertical displacement of ground surface given in Cai *et al.* (2011) with that of the present work, R_{E} = 1, R_{G} = 1 and R_{μ} = 1 is assumed, and other parameters of the track system and the ground are the same as with those of Cai *et al.* (2011). It can be seen that the results for the present work are in good agreement with the numerical result of Cai *et al.* (2011).

Table 1 Parameters of the train

P_{E} (kN)	P_{C} (kN)	L_{E} (m)	L_{C} (m)	w_{a} (m)	w_{b} (m)	d_{t} (m)	L_{Dis} (m)
162	120	22.2	24.4	2.9	14.8	4	-35

Table 2 Parameters of the slab track and ground soil

Track structure		The first layer				The second layer			
Parameter	Value	Parameter	Value	Parameter	Value	Parameter	Value	Parameter	Value
δ_{R} (N·m^2)	6.62E7	$E_{\mathrm{V}}^{(1)}$ (Pa)	3.0E7	$\rho_{\mathrm{f}}^{(1)}$ (kg·m^{-3})	1000	$E_{\mathrm{V}}^{(2)}$ (Pa)	5.0E7	$\rho_{\mathrm{f}}^{(2)}$ (kg·m^{-3})	1000
m_{R} (kg·m^{-1})	120	$E_{\mathrm{H}}^{(1)}$ (Pa)	5.0E7	$n^{(1)}$	0.3	$E_{\mathrm{H}}^{(2)}$ (Pa)	8.0E7	$n^{(2)}$	0.3
δ_{S} (N·m^2)	1.11E8	$\mu_{\mathrm{HH}}^{(1)}$	0.3	$\alpha^{(1)}$	0.9	$\mu_{\mathrm{HH}}^{(2)}$	0.3	$\alpha^{(2)}$	0.9
m_{S} (kg·m^{-1})	4000	$\mu_{\mathrm{HV}}^{(1)}$	0.3	$M^{(1)}$	2.45E9	$\mu_{\mathrm{HV}}^{(2)}$	0.3	$M^{(2)}$	2.45E9
k_{P} (N·s^{-1})	1.7E8	$G_{\mathrm{V}}^{(1)}$ (Pa)	1.5E7	$\eta_{\mathrm{w}}^{(1)}$ (Pa·s)	0.034	$G_{\mathrm{V}}^{(2)}$ (Pa)	3.0E7	$\eta_{\mathrm{w}}^{(2)}$ (Pa·s)	0.034
C_{P} (N·s·m^{-1})	1.24E5	$\rho^{(1)}$ (kg·m^{-3})	1816	$k_{\mathrm{s}}^{(1)}$ (m^3·s·kg^{-1})	1.0E-9	$\rho^{(2)}$ (kg·m^{-3})	1816	$k_{\mathrm{s}}^{(2)}$ (m^3·s·kg^{-1})	1.0E-9

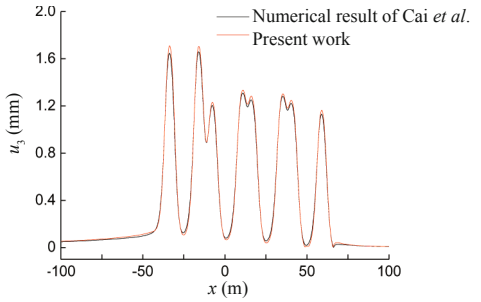

Fig. 3 Comparison between present work and that by Cai *et al.* (2011)

3.2 The influence of train load velocity

The train is assumed to move at c = 30 m/s and c = 50 m/s, which are far below the Rayleigh-wave velocity of the soil medium, and c = 80 m/s and c = 100 m/s, which are closer to the Rayleigh-wave velocity of the soil medium. There was a significant difference for dynamic displacement of the ground surface when the train load velocity is low or high, as shown in Fig. 4. For the low train velocity (c = 30 m/s and 50 m/s), the dynamic displacement of the ground soil is in accord with the geometric distribution form of the train load, and reaches maximum on the position where the axle load of the train impinges. The axle loads of the engine are significantly greater than those of the carriages, so the maximum dynamic displacement of the ground soil occurs beneath the train wheels of the engine. The same peak values tend to appear between the close and adjacent axle loads due to the existence of the slab track, which also leads to the redistribution of train load. As the load velocity increases from c = 30 m/s to c = 50 m/s, the peak dynamic displacement has no obvious change. However, when the load velocity increases from c = 80 m/s to c = 100 m/s, the peak dynamic displacement increases significantly, and the vibration near the wheel area becomes violent.

With the increase of train velocity, the displacement of the ground surface first increases slowly at the low train load velocity, and then increases rapidly and reaches its peak value when the train load velocity is close to the Rayleigh-wave velocity of the ground soil as shown in Fig. 5. The train load velocity corresponding to the peak of the displacement is known as the critical velocity. When the train velocity is close to the critical velocity, the vibration displacement of the surrounding ground rises to the peak value because energy caused by the interaction between wheel, rail track structure and ground soil can't escape to generate a resonance. For the train velocity which is higher than the critical velocity, the displacement of the ground surface decreases significantly with increasing train load velocity.

The dynamic displacement gradually decays with the depth, as shown in Fig. 6, and the dynamic influence becomes deeper with increasing train velocity. The upper part of the track roadbed is mainly affected by train load, which will require additional damping measures to reduce the vibration effect.

It is important to study the excess pore water pressure of the soil media before, during and after actual train passages, since it has considerable effect on the settlement of the ground. The excess pore water pressure at x = -35, y = 0 is measured, and the result is shown in Fig. 7. With increasing train load velocity, the excess pore water pressure increases significantly, more obvious at depths of 0.5–3.0 m, and reaches its peak at depths of 1.0–2.0 m. When the speed of the train is close to the critical velocity, the effect of the coupling of the fluid and the soil skeleton is significant for soil structure at high train velocities. Intense vibration of the soil produces a greater excess pore water pressure resulting

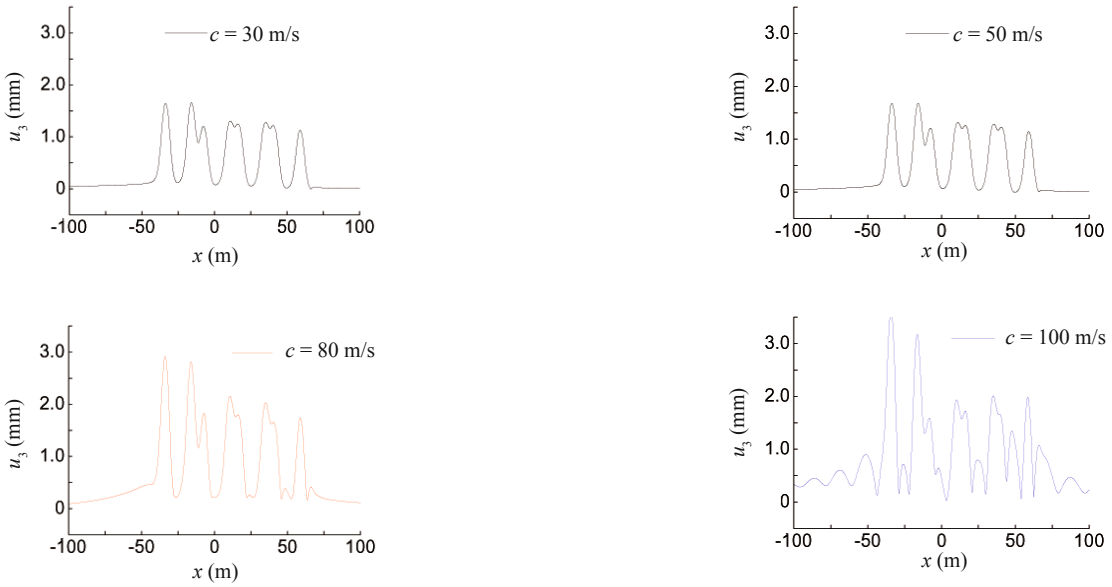

Fig. 4 Effect of load velocity on vertical displacement

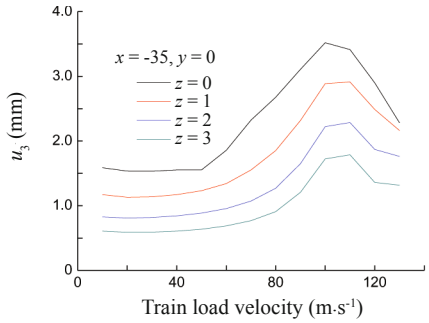

Fig. 5 Vertical displacement variation with train load velocity

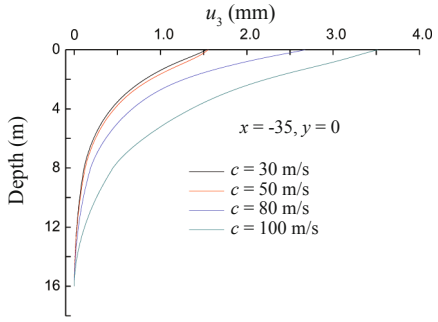

Fig. 6 Vertical displacement at different depth of ground

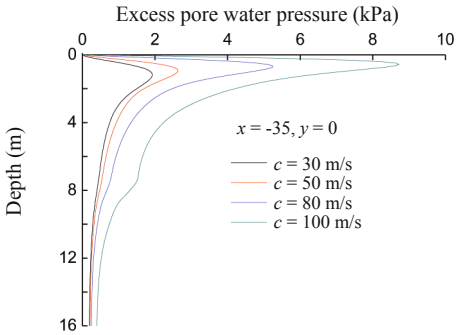

Fig. 7 Excess pore water pressure at different depth of ground

in soil softening. However, this only needs considering the pore water pressure in the vicinity of ground surface, because the peak of the excess pore water pressure is only within the first few meters.

3.3 The influence of transversely isotropic parameter

To investigate the elastic modulus effect, $R_E = E_H/E_V$ is defined to represent the degree of anisotropy of the modulus, and three conditions for R_E = 0.5, R_E = 1.0 and R_E = 2.0 are investigated and other parameters are kept the same as in Table 2. The results are shown in Figs. 8 and 9. The vertical displacement of the ground surface decreases with the increase in R_E. For the low train velocities, the variation of R_E has little effect on the displacement of ground soil, and the vertical displacement of the ground surface decreases from 1.85 mm to 1.47 mm as the R_E increases from 0.5 to 2.0 when c = 30 m/s. Whereas for the high train velocities, the change of R_E has a greater impact on the displacement of ground soil, and the vertical displacement of the ground surface decreases from 4.12 mm to 3.38 mm when c = 100 m/s. This means that the modulus ratio is larger, and the foundation is safer, especially under high train load velocities. The peak value of excess pore water pressure is little affected by R_E, but with increasing R_E, the distribution curve of pore water pressure becomes wider along the depth. This means that the region of excess pore water pressure becomes larger with the increase of the modulus ratio R_E. The traditional design method of the foundation assumes the ground soil is homogeneously isotropic, and considers only the impact of E_V. The method is suitable for low train velocities, but for high train velocities, it is satisfactory only when the actual soil $R_E > 1$ ($E_H > E_V$), but unsafe if $R_E < 1$ ($E_H < E_V$).

To investigate the shear modulus effect, $R_G = C_{66}/G_V$ is defined to represent the degree of anisotropy of the shear modulus, supposing R_G = 0.78, R_G = 1.0 and R_G = 1.3, respectively, and the other parameters are kept the same as in Table 2. The results are shown in Figs. 10 and 11. For the low train velocity when c = 30 m/s, like the effect of R_E, the variation in R_G has a small effect on the displacement. But for the high train velocity when c = 100 m/s, the change in R_G then has a significant effect on the dynamic response. The peak value of excess pore water pressure decreases and the distribution

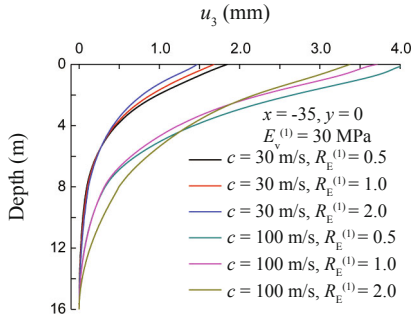

Fig. 8 Effect of $R_E^{(1)}$ on vertical displacement at different depth of ground

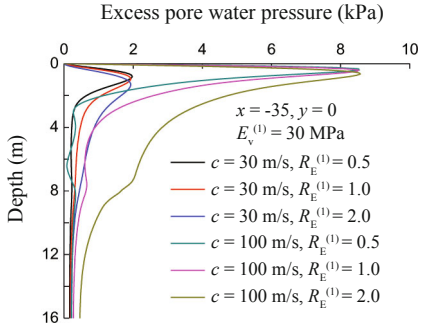

Fig. 9 Effect of $R_E^{(1)}$ on excess pore water pressure at different depth of ground

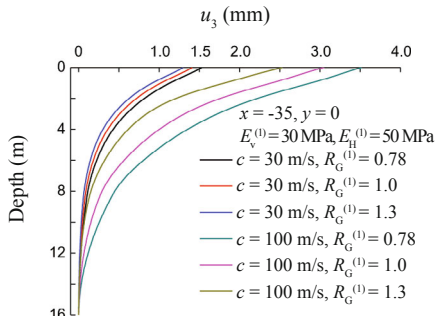

Fig. 10 Effect of $R_G^{(1)}$ on vertical displacement at different depth of ground

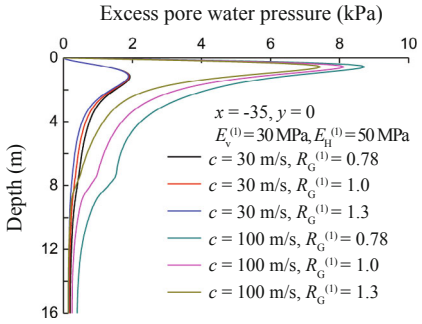

Fig. 11 Effect of $R_G^{(1)}$ on excess pore water pressure at different depth of ground

curves of which along the depth become thinner with the increases in R_G. With the traditional design method of the foundation under high train load velocities, if the actual soil $R_G > 1$, then using the conservative design method is adequate, while if $R_G < 1$, it is unsafe.

To investigate the effect of Poisson′s ratio, $R_\mu = \mu_{HH}/\mu_{HV}$ is defined, Figs. 12 and 13 show that whether for high or low train velocity, the effect of the displacement and excess pore water pressure is limited with the change of R_μ. The above analysis shows that the transversely isotropic properties of the foundation have a significant influence on the dynamic responses, especially under high train load velocities, and it needs to be emphasized and formally adopted in engineering practice.

3.4 The effect of anisotropic parameters of the subsoil layer

Figures 14 to 19 show that the calculated vertical displacement and excess pore water pressure varies with the anisotropic parameter of the subsoil layer, and that the anisotropic parameters of the surface layer have more effect on the vertical displacement and excess pore water pressure than those of the subsoil layer. The anisotropic parameters of the subsoil only have an influence on its own layer. Due to the limited dynamic influence of depth under train load, it is rational to control ground vibration of train loads by raising the stiffness of the upper soil layer.

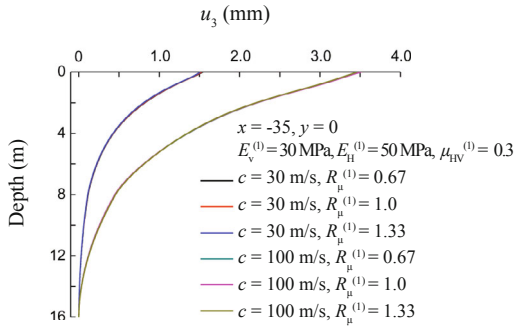

Fig. 12 Effect of $R_\mu^{(1)}$ on vertical displacement at different depth of ground

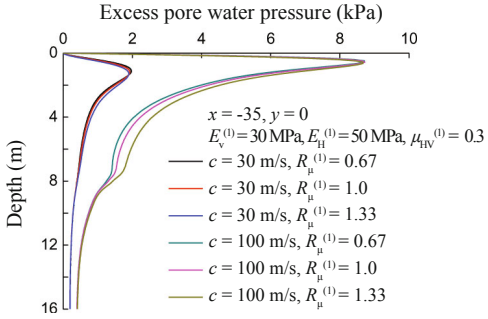

Fig. 13 Effect of $R_\mu^{(1)}$ on excess pore water pressure at different depth of ground

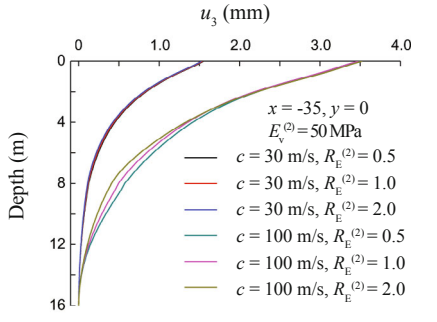

Fig. 14 Effect of $R_E^{(2)}$ on vertical displacement at different depth of ground

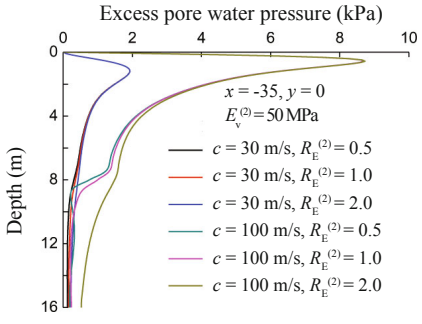

Fig. 15 Effect of $R_E^{(2)}$ on excess pore water pressure at different depth of ground

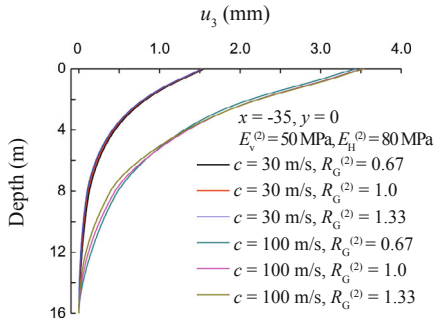

Fig. 16 Effect of $R_G^{(2)}$ on vertical displacement at different depth of ground

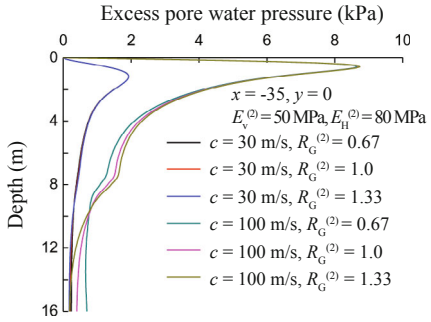

Fig. 17 Effect of $R_G^{(1)}$ on excess pore water pressure at different depth of ground

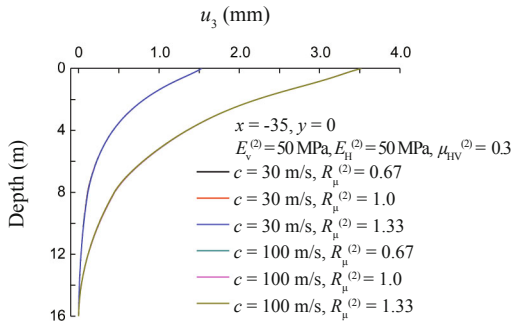

Fig. 18 Effect of $R_\mu^{(2)}$ on vertical displacement at different depth of ground

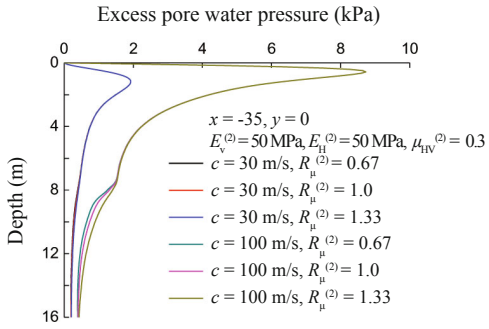

Fig. 19 Effect of $R_\mu^{(2)}$ on excess pore water pressure at different depth of ground

4 Conclusions

In this work, the dynamic responses of slab tracks on multi-layered transversely isotropic saturated soils subjected to train loads were investigated using the Fourier transform, and the FFT (Fast Fourier Transform) procedure was employed to calculate the inverse Fourier transform. The main conclusions are as follows:

(1) The distribution of the vertical displacement response is quite different along the longitudinal line under low and high train velocities. The amplitude of surface displacement first slowly increases with increasing train velocity, and then sharply increases and reaches its peak value when the velocity is close to the critical velocity. As the train velocity increases beyond the critical velocity, the displacement rapidly decreases with the increasing train velocity.

(2) The transverse isotropy and the characteristics of layered soils have a remarkable influence on the vertical displacements for high train velocities. The amplitude of vertical displacement of the ground surface decreases with the increasing anisotropic parameters of R_E and R_G. The anisotropic parameters of the surface soil layer have a greater influence on the displacement and excess pore water pressure than those of the subsoil layer. It is rational to control ground vibration induced by train loads by raising the stiffness of the upper soil layer.

(3) The amplitude of excess pore water pressure increases with increasing load velocity, and the anisotropic parameters of ground soil have a greater influence on excess pore water pressure for high train velocities. However, excess pore water pressure only needs consideration in the vicinity of ground surface, because the peak inexcess pore water pressure is only within the first few meters.

(4) With the traditional design method of the foundation, it is assumed that ground soil is homogeneous isotropic soil and does not consider the transverse isotropy, which may lead to unsafe calculation results for the case of $R_E < 1$ and $R_G < 1$. Therefore, the transverse isotropic foundation model is of great significance for designing high speed railway.

Acknowledgement

This research is supported by the National Basic Research Program of China (No. 2013CB036405), the Key Research Program of the Chinese Academy of Sciences (No. KZZD-EW-05) and the Natural Science Foundation of China (Nos. 41402317, 51209201 and 51279198). These financial supports are gratefully acknowledged.

References

Abouseiman Y and Cui L (1998), "Poroelastic Solutions in Transversely Isotropic Media for Wellbore

and Cylinder," *International Journal of Solids arid Structures*, **35**(35): 4905–4929.

Bian Xuecheng, Jiang Hongguang and Chen Yunmin (2010), "Accumulative Deformation in Railway Track Induced by High-speed Traffic Loading of the Trains," *Earthquake Engineering and Engineering Vibration*, **9**: 319–326. (in Chinese)

Biot MA (1956), "Theory of Propagation of Elastic Waves in a Fluid-saturated Porous Solid. Part I: Low-frequency Range; Part II: High-frequency Range," *Journal of the Acoustical Society of America*, **28**: 168–191.

Biot MA (1962), "Mechanics of Deformation and Acoustic Propagation in Porous Media," *Journal of Applied Physics*, **33**: 1482–1498.

Burke M and Kingsbury HB (1984), "Response of Poroelastic Layers to Moving Loads," *International Journal of Solids and Structures*, **20**: 499–511.

Cai YQ, Sun HL and Xu CJ (2008), "Three Dimensional Analysis of Dynamic Responses of Track Ground System Subjected to a Moving Train Load," *Computers and Structures*, **836**: 816–824.

Cai Yuanqiang, Wang Yu and Cao Zhigang (2011), "Dynamic Analysis of a Slab Track on the Poroelastic Soil Subjected to Moving Loads," *Journal of Vibration Engineering*, **24**(1): 48–54. (in Chinese)

Chen Guangjing, Zhao Xihong and Yu Li (1998), "Transferring Matrix Method for Solutions of Non-axisymmetric Load Applied to Layered Cross-anisotropic Elastic Body," *Chinese Journal of Geotechnical Engineering*, **26**(5): 522–527. (in Chinese)

Jin Bo (2004), "Dynamic Response of a Poroelastic Half Space Generated by High Speed Load," *Chinese Quarterly of Mechanics*, **25**: 168–174. (in Chinese)

Kennedy TC and Herrmann G (1973a), "Moving Load on a Fluid-solid Interface: Subsonic and Intersonic Regimes," *Journal of Applied Mechanics*, **40**: 885–890.

Kennedy TC and Herrmann G (1973b), "Moving Load on a Fluid–solid Interface: Supersonic Regimes," *Journal of Applied Mechanics*, **40**:137–142.

Ling Xianzhang, Zhang Feng, Zhu Zhanyuan, Ding Lin and Hu Qingli (2009), "Field Experiment of Subgrade Vibration Induced by Passing Train in a Seasonally Frozen Region of Daqing, "*Earthquake Engineering and Engineering Vibration*, **8**: 149–157. (in Chinese)

Lu JF and Jeng DS (2007), "A Half-space Saturated Poro-elastic Medium Subjected to a Moving Point Load," *International Journal of Solids and Structures*, **44**: 573–586.

Picoux B and Le Houedec D (2005), "Diagnosis and Prediction of Vibration from Railway Trains," *Soil Dynamics and Earthquake Engineering*, **25** (12): 905–921.

Rahman M and Newaz G (2000), "Boussinesq Type Solution for a Transversely Isotropic Half-space Coated with a Thin Film," *International Journal of Engineering Science*, **38**(7): 807–822.

Siddharthan R, Zafir Z and Norris GM (1993), "Moving Load Response of Layered Soil. I: Formulation; II: Verification and Application," *Journal of Engineering Mechanics*, ASCE, **119** (10): 2052–2089.

Takemiya H and Bian XC (2005), "Substructure Simulation of Inhomogeneous Track and Layered Ground Dynamic Interaction under Train Passage," *J. Eng. Mech*., **131**: 699–711.

Theodorakopoulos DD (2003), "Dynamic Analysis of a Poroelastic Half-plane Soil Medium under Moving Loads," *Soil Dynamics and Earthquake Engineering*, **23** (7): 521–533.

Wang CD, Pan E, Tzeng CS, Han F and Liao JJ (2006), "Displacements and Stresses due to a Uniform Vertical Circular Load in an Inhomogeneous Cross-anisotropic Half-space," *International Journal of Geomechanics*, **6**(1): 1–10.

Yu HY (2001), "A Concise Treatment of Indentation Problems in Transversely Isotropic Half-space," *International Journal of Solids and Structures*, **38**(10): 2213–2232.

Yue ZQ (1995), "Elastic Fields in Two Joined Transversely Isotropic Solids due to Concentrated Forces," *International Journal of Engineering Science*, **33**(3): 351–369.